

Variable porous structure of laser-ablated silicon nanocluster films and its influence on photoluminescence properties

A. V. Kabashin*, J.-P. Sylvestre, S. Patskovsky, M. Meunier

Ecole Polytechnique de Montréal, Département de Génie Physique, Case Postale 6079, succ. Centre-ville, Montréal (Québec), Canada, H3C 3A7

ABSTRACT

Si/SiO_x films were fabricated by Pulsed Laser Ablation from a silicon target in a residual gas. The films were crystalline with minimal grain size of 2-4 nm and had a porous morphology. The film structure was found to be extremely sensitive to deposition conditions with porosity depending on the gas pressure during the deposition. In particular, the increase of helium pressure from 0.2 to 4 Torr in different depositions led to a gradual porosity (P) increase from 10% to 95%. The porosity increase was accompanied by a slight increase of mean crystal size in the deposit. It has been established that photoluminescence (PL) properties were different for films with different porosities. For low porous films (P < 40 %), we observed PL signals with peak energies between 1.6 and 2.12 eV depending on helium deposition pressure. In contrast, PL properties of highly porous films (P > 40%) were mainly determined by post-deposition oxidation phenomena. They led to an enhancement of PL bands around 1.6-1.7 eV and 2.2-2.3 eV, which were independent of deposition conditions. Similar 2.2-2.3 eV signals were observed after strong film oxidation through a thermal annealing of films in air or through a silicon ablation in oxygen-containing atmosphere. Mechanisms of film formation and PL origin are discussed.

Keywords: pulsed laser ablation, silicon, nanocluster film, photoluminescence, porosity.

1. INTRODUCTION

The expansion of Si-based technologies to optoelectronics has been limited for a long time by the fact that bulk silicon has an indirect and small (1.11 eV at room temperature) band gap. However, recent observations of visible photoluminescence (PL) at room temperature from porous silicon and various nanostructured Si-based films enable to reexamine the optoelectronics application of silicon-contained materials and give a promise for the creation of silicon-based optoelectronics devices.

Pulsed Laser Ablation (PLA) is a “dry” deposition technique, which is widely used for the fabrication of silicon-based nanocrystallites. PLA makes possible a fine variation of the nanocluster parameters during the deposition^{1,2} and a formation of Si/SiO_x nanostructured films exhibiting visible PL (see, e.g., Refs. 3-11). The appearance of PL is generally related to the presence of nanoscale crystals in the deposit, while different mechanisms such as quantum confinement effect¹², surface radiation states¹³, defects in Si₂ structure¹⁴ etc. are considered to explain PL characteristics. However, PL properties from laser-ablated films were not similar in different studies. Some groups reported nearly fixed PL peaks around 1.5-1.7 eV and 2.1-2.2 eV for the films deposited under different conditions⁴⁻⁸, whereas other teams observed a clear shift of PL peak when the particle size was changed by a variation of deposition parameters⁹. In our opinion, such difference in photoluminescence properties may be connected to not only to different ablation parameters, but to different post-deposition conditions as well. For example, in some studies⁵⁻⁸ the films were thermally annealed after the fabrication, that could additionally modify their properties. We believe that to get better understanding of the PL origin, one must clearly separate the contribution from the laser ablation itself and from the post-deposition conditions. In addition, we suppose that a correlation of PL properties with grain size is not sufficient to explain all variety of PL

* akabach@email.phys.polymtl.ca; phone 1-(514)340-4711 ext. 4634, Ecole Polytechnique de Montréal, Département de Génie Physique et Groupe de recherche en physique et technologie des couches minces (GCM), Case Postale 6079, succ. Centre-ville, Montréal (Québec), Canada, H3C 3A7

characteristics. Other parameters such as e.g. film morphology and chemical composition should as well be taken into consideration.

In this paper, we compare properties of as-deposited and post-oxidized films and thus identify PL peaks related to different phenomena. The main attention is given to the visible and near-infrared ranges of the spectrum (S-band), which are the most important for optoelectronics applications.

2. EXPERIMENTAL SETUP

The ablation of material from a rotating Si target ((1-0-0), N-type, resistivity 10 Ohm-cm) was produced by a pulsed KrF laser ($\lambda = 248$ nm, pulse length 15 ns FWHM, repetition rate 30 Hz). The radiation was focused on a focal spot 2×1 mm² on the target at the incident angle of 45° as shown in Fig. 1. The fluence was $7-10$ J/cm² giving a radiation intensity of about $5 \cdot 10^8$ W/cm². The laser-induced plasma plume expanded perpendicularly to the target surface. The substrates, identical to the target, were placed on a rotating substrate holder at 2 cm from the target. Both the target and the substrate were kept at room temperature. The deposition was carried out in He (purity 99.9995%) at a constant ambient pressure. The pressure P of He was varied in different experiments between 50 mTorr and 10 Torr, while the laser pulse energy and target-to-substrate distance were fixed. The chamber was pumped down to $P = 2 \cdot 10^{-7}$ Torr before filling with the gas. Under the residual air pressure of $2 \cdot 10^{-7}$ Torr and the laser repetition rate of 30 Hz, oxidation of ablated silicon layers is negligible between the laser pulses⁹. After several thousand laser shots, the thickness of the Si film on the substrate was 100 – 1000 nm. For some comparative tests, the deposition was also performed in pure oxygen. The pressure of oxygen did not exceed 200 mTorr in order to maintain a relatively intense plasma plume.

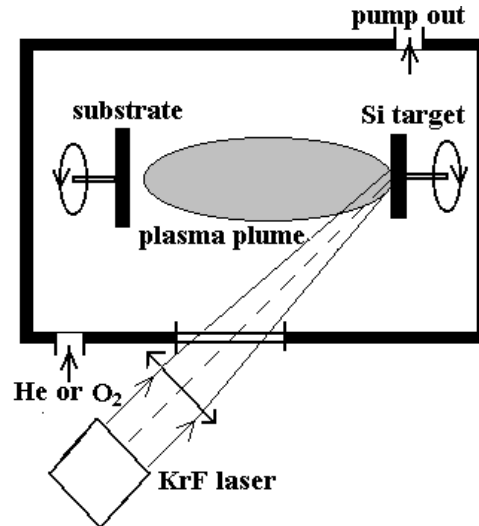


Fig. 1 Experimental arrangement

In addition, a technique of thermal evaporation from a Si target in vacuum has been used for comparative tests. In contrast to PLA, this technique is known to provide amorphous films with relatively large dimensions of deposited particles. A powder from a Si wafer with the same parameters was evaporated under the residual pressure of 10^{-7} Torr from a tantalum boat onto a Si substrate maintained at room temperature. The boat to substrate distance was about 15 cm, the deposition rate was 0.1-0.2nm/s as measured by a quartz microbalance system. The thickness of deposited amorphous Si films on the substrate was 100-200 nm. In some cases, the films deposited by PLA and thermal evaporation were annealed at 800° C in atmospheric air for 10 minutes. The increase and decrease rates of temperature were 10° C/min.

For the photoluminescence measurements, the samples were illuminated by the radiation of cw Ar⁺ laser (model INNOVA 100) with the wavelength 488 nm. The power was 10 mW and the power density on the analyzed samples was

estimated to be 30 W/cm^2 . The PL spectra were measured at room temperature using a double spectrometer (model U100, Instruments SA) and GaAs photomultiplier (Hamamatsu Photonics). The spectra were corrected to take into account the spectral response of the PL setup.

Scanning Electron Microscopy (SEM), Atomic Force Microscopy (AFM) were used to examine the morphology of laser-ablated films. The crystallinity of the films was studied by X-ray diffraction (XRD) spectroscopy, while the film porosity was estimated from Specular X-ray Reflectivity¹⁵ (SXRR) measurements. To determine the composition of the surface layer, the films were also analyzed by X-ray Photoemission Spectroscopy (XPS) at a base pressure of $2 \cdot 10^{-8}$ Torr, using a Thermo VG Scientific system.

3. STRUCTURAL PROPERTIES OF LASER-ABLATED FILMS

3.1 AFM study

These experiments were carried out to estimate dimensions of silicon clusters produced by the pulsed laser ablation process. A fraction of a monolayer of clusters was deposited on a substrate of highly oriented pyrolytic graphite (HOPG), which is known to have an atomically flat surface. The size of the particles was recorded by the AFM technique in the “tapping” mode. A profile analysis of an AFM image of several isolated laser-ablated particles is shown in Fig. 2(a). One can see that the height of the particles was about 2-4 nm, while their recorded lateral dimensions were about 20-30 nm. It is known that real size of nanoobjects is truly presented only by the height measurements, while their lateral dimensions are usually enlarged due to the tip-object convolution effect. Therefore, we may conclude that the real size of the smallest ablated particles was about 2-3 nm, which is in agreement with previous studies of laser-ablated Si-based deposits by Transmission Electron Microscopy (4-10 nm)⁵ and Atomic Force Microscopy (1-10 nm)^{6,9,16} techniques. However, larger particles with dimensions of about 10-15 nm were also present in some images. Performing the depositions under different helium pressures, we were able to clarify the influence of the pressure on the mean nanoparticle size. As shown from Fig. 2(b), the mean size increased with helium pressure, though the size variations did not exceed 1 nm. This is also in good agreement with pressure dependence of mean nanocrystal size reported in previous studies^{5,16}.

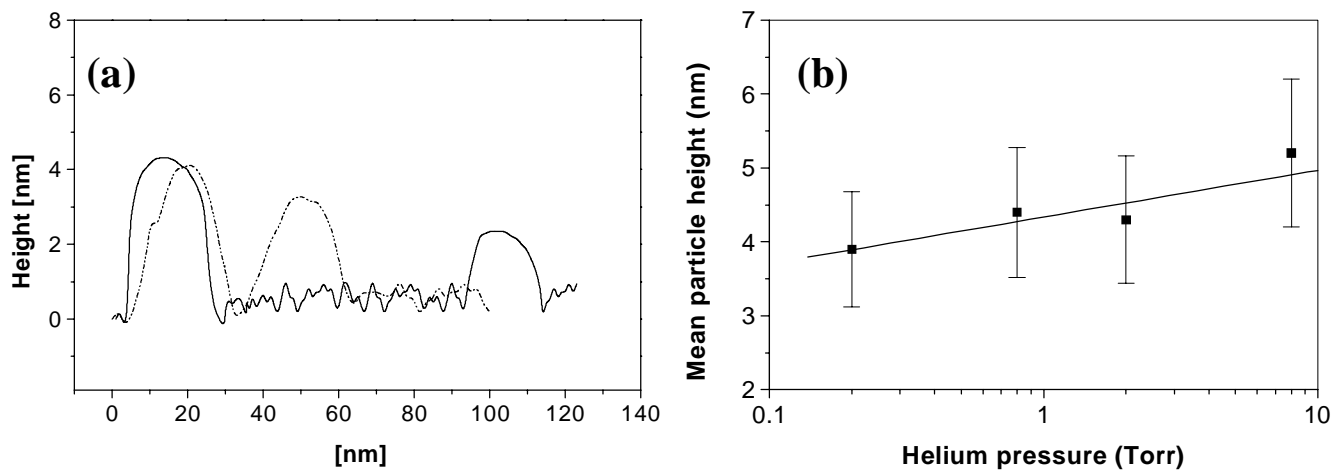


Fig. 2 (a) Profile analysis of the AFM image of isolated laser-ablated particles on graphite (HOPG) substrate; (b) Mean particle height from AFM images as a function of helium pressure during the deposition

3.2 SEM study

As follows from SEM images presented in Fig. 3, the morphology of laser-ablated films was very sensitive to a residual gas pressure during the deposition process. While only initial signs of roughness were discerned with the films deposited under 1 Torr, the experiment under 2 Torr provided a developed porous structure with pore size of about 50-100 nm.

Further pressure increase up to 4 Torr led to a formation of web-like aggregations of particles. Note that under $P < 1$ Torr the roughness details were too small to be detected by our SEM system. Thus, our experiments clearly show that not only the mean particle size, but also the morphology of the films depends on the deposition conditions.

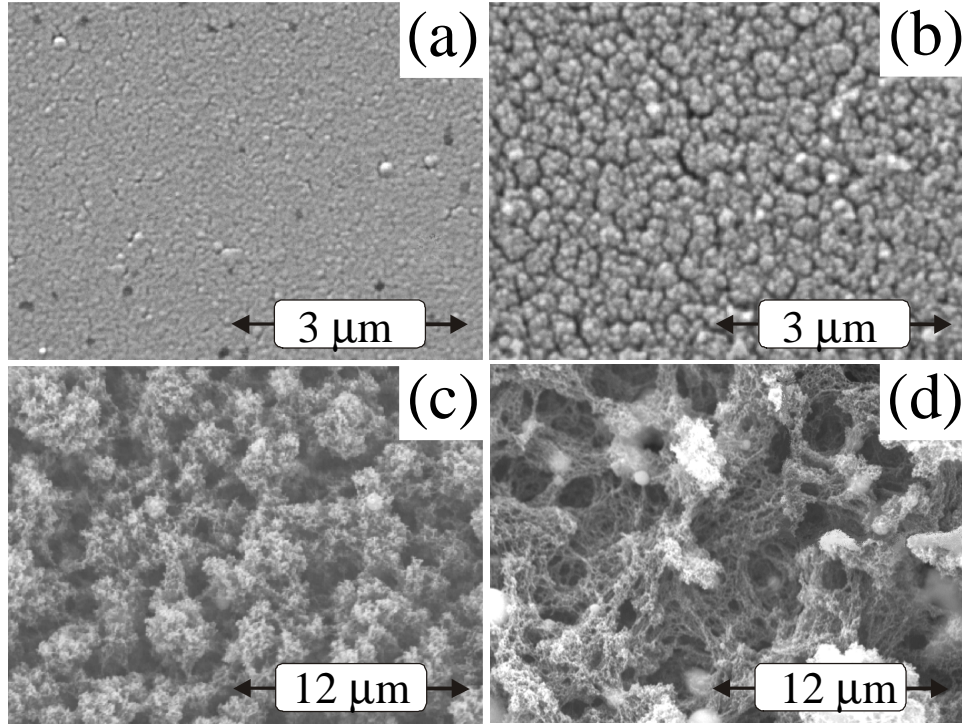


Fig. 3 SEM images of the laser-ablated films fabricated under 1 Torr (a), 2 Torr (b), 4 Torr (c), 8 Torr (d).

3.3 SXRR measurements

The porosity of the laser-ablated films was estimated from Specular X-ray Reflectivity (SXRR) measurements¹⁵. SXRR spectra were obtained with the use of a simple powder X-ray diffractometer, which made possible a monitoring of the intensity of an X-ray beam reflected from a surface under a simultaneous θ - 2θ scanning of a source and a detector ($0^\circ < \theta < 1^\circ$, θ was measured towards the surface). Since for X-rays the refractive index of most materials is less than 1, a phenomenon of total external reflection occurs for $\theta < \theta_c$, while for $\theta > \theta_c$ the reflected intensity suffers a rapid attenuation. Because θ_c is proportional to the square root of the electronic density, which is directly proportional to the density of the material, the experimental determination of the critical angle gives access to the density of the material. For a given material, a porosity increase results in a density decrease, which can be quantified by a decrease of the critical angle as follows:

$$porosity(\%) = 100 \left(1 - \frac{\theta_c^2}{\theta_{c, bulk Si}^2} \right) \quad (1)$$

where θ_c and $\theta_{c, bulk Si}$ are the critical angles from SXRR spectra for a thin film and bulk silicon, respectively.

Experimental reflectivity curves for a silicon substrate (wafer) with and without laser-ablated films are presented in Fig. 4 (a). One can see that the critical angle for the substrate $\theta_{c, bulk Si}$ was about 0.22° . Similar substrate-related angle of 0.22° could be observed for samples with laser-ablated films as shown in Fig. 4 (a). However, the later samples also contained an additional air/film interface-related critical angle θ_c , whose position depended on helium pressure. For example, for

the films deposited at 0.5 Torr and 2 Torr, we had $\theta_{c1} = 0.19^\circ$ and $\theta_{c2} = 0.11^\circ$, respectively [Fig. 4 (a)]. Substituting the values of θ_{c1} and θ_{c2} into equation (1), we obtain the film porosities of 25% and 75%, respectively.

Fig. 4 (b) summarizes the porosity measurements for laser-ablated films deposited under different pressures P. Here, a tendency of the porosity enhancement with the pressure increase is quite clear for $P < 2$ Torr, while for higher pressures the porosity always exceeds 95%. It is necessary to note that the precision of SXRR measurements was about 10%.

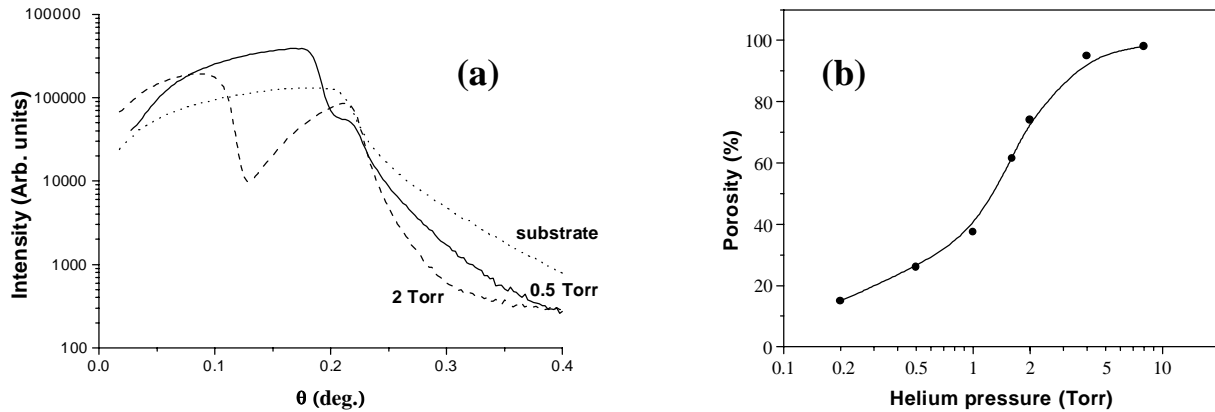


Fig. 4 (a) Typical SXRR curves for a silicon wafer (substrate) and laser-ablated films fabricated at 0.5 and 2 Torr of helium. (b) Porosity of the films estimated from SXRR curves as a function of helium pressure during the deposition.

3.4 XRD study

As shown in Fig. 5, XRD spectra of the laser-ablated films exhibited all peaks typical for crystalline silicon. In addition, an analysis of XRD spectra of some samples deposited at reduced pressures $P = 0.2-0.5$ Torr indicated the presence of a minor amorphous phase.

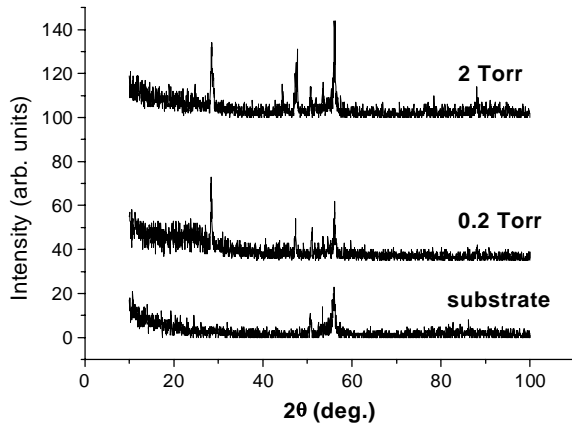


Fig. 5 Typical X-ray Diffraction spectra from silicon substrate and laser-ablated films fabricated at 0.2 and 2 Torr of helium.

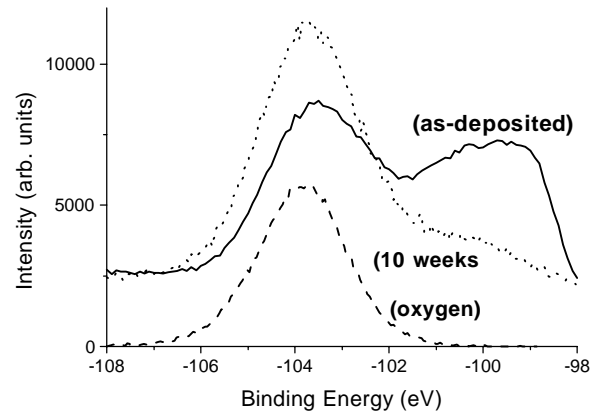


Fig. 6 Typical XPS spectra from the films prepared by laser ablation under 2 Torr of helium just after their fabrication (as-deposited) and after 10 weeks of their exposition to ambient air (10 weeks). (oxygen) – Typical XPS spectrum of the film deposited under 0.15 Torr of oxygen.

3.5 XPS study

The surface composition of the films was examined by X-ray Photoelectron Spectroscopy (XPS). Fig. 6 shows the XPS spectra of a film just after its fabrication (spectrum “as-deposited”) and after 8 weeks of its exposition to ambient air (“10

weeks”). The spectrum of the as-deposited sample demonstrates two peaks at about 99.8 and 103.2 eV, which are assigned to the Si 2p photoelectrons of the unoxidized Si core and the SiO_x oxide layer, respectively. The spectrum of the oxidized sample (10 weeks) reveals a decrease of the low-energy peak with a slight shift to higher binding energies. On the other hand, the high-energy peak becomes stronger and shifts to higher energies up to 104 eV, which is assigned to 2p photoelectrons of pure SiO₂. Our XPS results shown in Fig. 6 suggest that the composition x of the surface oxide increases as the exposition time increases. For the comparison, we also analyzed XPS spectra of the films deposited in pure oxygen. In this case, we only observed the peak at about 104 eV (spectrum “oxygen”), which corresponds to the photoelectrons of pure SiO₂. Similar spectrum was observed after that the thermal annealing of the films deposited in helium, suggesting that the annealing led to an extensive film oxidation.

4. PHOTOLUMINESCENCE PROPERTIES

4.1 As-deposited films

The films deposited under different helium pressures showed quite different PL characteristics. For films deposited at reduced pressures $P < 1.5$ Torr, we recorded PL spectra, whose peak energy positions strongly depended on the pressure. The pressure dependencies for peak energy position and integral intensity of the PL signals are presented in Fig. 7. One can see that a pressure increase from 0.15 to 1.5 Torr in different depositions caused a red shift of the peak from 2.12 eV to 1.6-1.7 eV (curve (1)). However, for films deposited at relatively high pressures $P > 1.5$ Torr we observed quite different PL signals. The peak energy of these signals was always around 1.6-1.7 eV and did not depend on helium pressure during the deposition. In addition, the intensity of 1.6-1.7 eV signals was much stronger, while the most efficient PL was reported with the films deposited at 2 Torr (curve (2)).

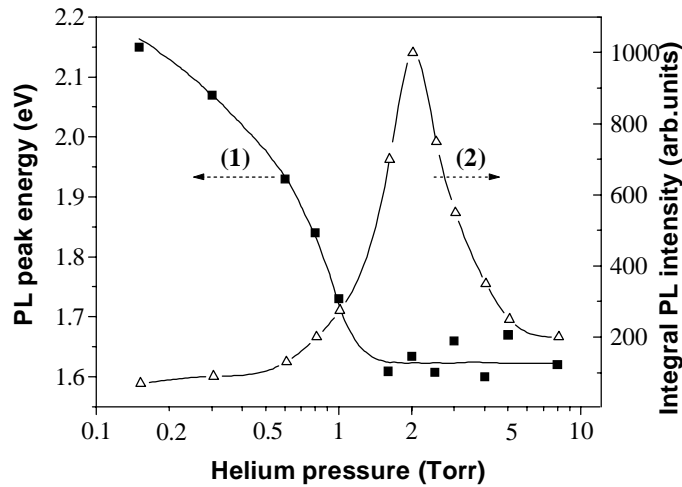


Fig. 7. PL peak energy (1) and integral PL intensity (2) as a function of the helium pressure for as-deposited films.

4.2 Prolonged natural oxidation

We found that oxidation phenomena could lead to a dramatic modification of PL properties from laser-ablated films. First of all, we observed a considerable enhancement of integral intensity of 1.6-1.7 eV signals under a prolonged storage of the films in pure dry air as shown in Fig. 8(a). The intensity could increase by a factor of 4-10 and stabilized only after 8-12 weeks, while the increase rate depended on the relative air humidity. The enhancement was accompanied by a slight red shift of the peak energy position as shown in Fig. 8(a). It is necessary to note that the 1.6-1.7 eV signals were recorded only with films deposited at relatively high helium pressures $P > 1.5$ Torr. These films were characterized by a relatively high porosity, exceeding 40% [Fig. 4 (b)]. Fig. 8 (b) presents the dependence of the integral intensity of the PL signals on film porosity. One can clearly see that only highly porous films demonstrated PL intensity enhancement. On the other hand, blue-shifted PL signals from low porous films remained stable even after their prolonged storage in air.

Secondly, we observed an appearance of an additional PL peak at about 2.2-2.3 eV under a prolonged storage of porous samples (with porosity higher than 40%) in humid air environment (relative humidity 80-100%), as shown in Fig. 8 (a) (spectrum “humid”). It is important to mention that the appearance and enhancement of 1.6-1.7 eV and 2.2-2.3 eV components correlated well with the relative increase of x in oxygen-related SiO_x complexes ($0 < x < 2$) of the upper film layer, as measured by XPS [Fig. 6]. This correlation between spectral and surface composition modifications gives evidence for oxidation-related origin of these components.

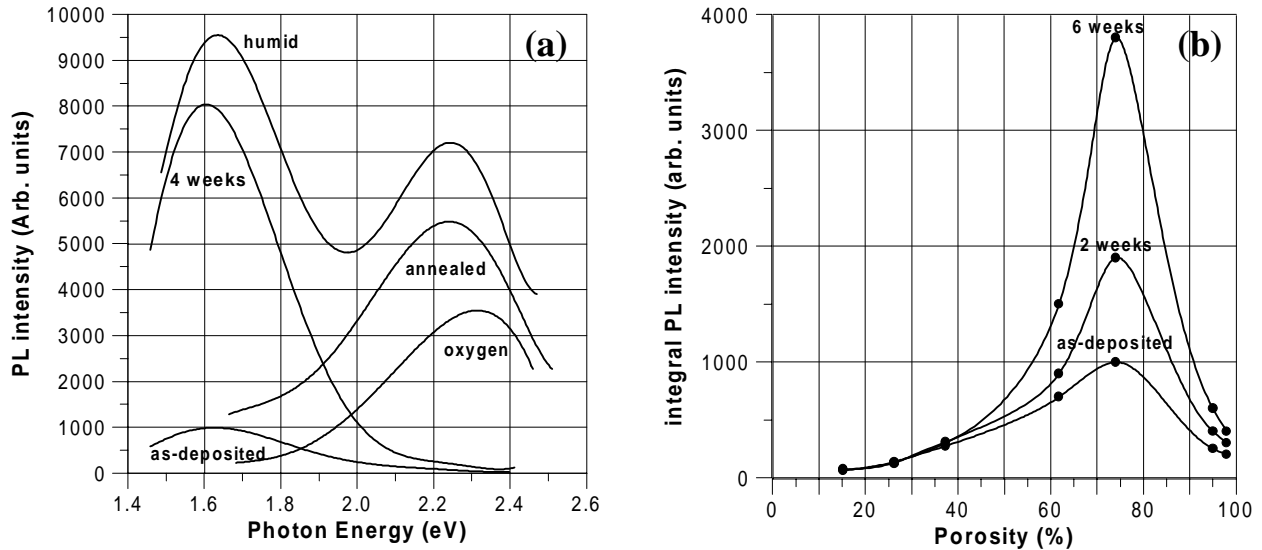


Fig. 8 (a) Photoluminescence spectra from Si/SiO_x films deposited by PLA under P = 2 Torr of helium: as-deposited, after 4 weeks of film storage in dry air; after 8 weeks of the of the storage in humid air (humid); after thermal annealing in air (annealed); (oxygen) - PL spectrum from films deposited in oxygen.

(b) Integral intensity of PL signals as a function of film porosity under a prolonged storage of the films in dry air.

4.3 Thermal oxidation

Similar dramatic modification of PL properties was observed after the profound oxidation of the films deposited in helium. It was produced by the annealing of the films in air at 800 °C (10 min). The thermal annealing resulted in the appearance of a single peak around 2.2-2.25 eV for all films prepared under different helium pressures, as shown in Fig. 8(a) (spectrum “annealed”). Moreover, the annealing of relatively old samples led to a considerable decrease or even the disappearance of the 1.6-1.7 eV peak. It is interesting to note that the Si-based films, deposited by thermal evaporation from a Si target in vacuum, also exhibited 2.2-2.3 eV PL after the thermal annealing, though these films were not photoluminescent just after the fabrication and a prolonged exposition to ambient air. Such a coincidence of PL peak positions gives a clear evidence for similar final structures of thermally annealed particles for the films deposited by different methods. It is logical to conclude that these structures are mainly formed during the post-deposition thermal oxidation process.

4.4 Deposition in oxygen-containing atmosphere

Similar 2.2-2.3 eV signals were recorded for the laser-ablated films fabricated in oxygen-containing atmosphere. In particular, this peak was observed for all films deposited under different pressures of pure oxygen as shown in Fig. 8 (a) (spectrum “oxygen”). In contrast to the PLA in helium, the PL signals could be observed immediately after the deposition process, while a prolonged film exposition to air did not result in any detectable increase of the PL intensity. Nevertheless, PL signals from oxygen-deposited films were less intense than that of the He-deposited films by almost an order of magnitude.

5. DISCUSSION

Our experiments showed that film porosity is very sensitive to the ablation conditions. Even minor variations of the gas pressure during deposition cause a dramatic porosity change. This phenomenon is probably connected to different conditions of nanocluster film formation in the cases of low and high gas pressures. Collisions with light helium atoms cause a cooling of the clusters and their size enlargement. We believe that under relatively low pressures a number of collisions are not sufficient to condense and crystallize the clusters in gaseous phase. Therefore, the clusters in the gas phase are relatively hot and crystallize when they arrive on the substrate forming a dense and well-packed crystalline film, as one can see in Fig. 3(a). Under high pressures, more frequent collisions lead to a fast cooling and more effective condensation of clusters in the gaseous phase. As a result, they arrive on the substrate being partially crystallized and having an arbitrary shape, which causes a formation of highly porous layers and even web-like agglomerations, as shown in Fig. 3 (c,d).

We propose that it is the microstructure difference that causes the dramatic distinction of long-term PL properties for the films deposited at low and high pressures. Dense and self-coagulated structures of the films fabricated under $P < 1$ Torr minimize the impact of ambient atmosphere on the film properties. Indeed, we did not detect any remarkable changes of PL spectra even after a prolonged natural oxidation of low porous films [Fig. 8 (b)]. We believe that PL mechanism related to core silicon crystals are predominant for these films, though the upper surface oxide can also play a certain role in a formation of PL centers. In particular, the red shift of the spectra under an increase of helium residual pressure could be due to the quantum confinement mechanism¹². In this case, an air passivation of the nanoclustered film is necessary to saturate dangling bonds, thus reducing nonradiative recombination channels. This supposition is confirmed by the increase of mean particle height on AFM images with the increase of helium pressure [Fig. 2 (b)]. Nevertheless, other mechanisms may not be ruled out completely.

The porosity enhances the surface area, which is subjected to surface chemistry modifications due to interactions of nanocrystallites with oxygen and another elements or impurities in ambient air. This can dramatically enhance the role of oxidation in formation of PL centers and in particular relative contribution of oxygen-related PL mechanisms. Indeed, we recorded a considerable enhancement of 1.6-1.7 eV signals and appearance of additional 2.2-2.3 eV signals under prolonged natural oxidations of highly porous films in air [Fig. 8 (a)]. Strong oxidation caused by a thermal annealing of the films or direct silicon ablation in oxygen also led to the generation of 2.2-2.3 eV signals. It should be noted that similar components were observed in many previous studies with the use of various fabrication techniques (see, e.g., Refs. 13, 14, 17, 18). The origin of 2.2-2.3 eV PL seems to be relatively clear since it was thoroughly examined in some previous studies of highly oxidized porous silicon¹⁴ and various Si-based films (see, e.g., Refs. 17, 18). This component was unambiguously attributed to a radiative recombination through defects in SiO₂ structure such as the nonbridging oxygen hole centers^{14,19}. The defects are formed in oxygen-related silicon compounds, in particular under the thermal annealing¹⁴ or a prolonged film exposition to air¹⁸. In our experiments, the 2.2-2.3 eV component was also recorded after the thermal annealing in air, a prolonged humid oxidation of some films deposited in helium, and direct deposition of silicon in pure oxygen. We suppose that the 2.2-2.3 eV PL centers are effectively formed under a strong oxidation of Si-based films, which was the common feature of these cases.

A gradual growth of the integral intensity of 1.6-1.7 eV signals with time of the film prolonged exposition to air also gives an evidence for a contribution of oxygen in a formation of the PL signals. Similar phenomenon was recorded on films, deposited in an oxygen-free atmosphere by a laser decomposition of silane^{13,20}. However, there is no common consensus on the origin of these signals in the literature. Taking account the size-independent behavior of the 1.6-1.7 eV signals, some authors attribute it to a recombination through an interfacial layer between the c-Si core and the a-SiO₂ surface layer¹³. On the other hand, some properties of the red components such as a relatively long decay, enable to ascribe it to the quantum confinement mechanism (see, e.g., Refs. 21).

It is clear that in normal conditions, oxidation-related mechanisms give the strongest contribution when integral surface area of the film is maximal, but the pores give however enough access to inner film layers for oxygen and other elements. This compromise was probably achieved under 65-80% porosity, which led to the most efficient modification of PL characteristics with storage time in air and the strongest signals of 1.6-1.7 eV and 2.2-2.3 eV components.

Finally, we can not exclude that the mentioned discrepancy of experimental results related to the presence⁹ or absence⁵⁻⁸ of size dependence for PL spectra was because of different film microstructures in different studies. Relatively porous films could provide better conditions for oxidation-related mechanisms, while low porous films contributed to preferential contribution of another mechanisms, e.g., the quantum confinement one. In any case, our studies show that the film morphology must be taken into account in the interpretation of experimental results to avoid possible ambiguities and misunderstandings.

6. CONCLUSIONS

A method of pulsed laser ablation in a residual gas has been used to synthesize Si/SiO_x nanostructured films. We showed that porous microstructure can strongly affect the PL properties of the laser-ablated films. The low-porous film structure minimizes the effect of post-deposition natural oxidation on PL properties. In this case, PL signals with peak energies between 1.6 and 2.15 eV depending on helium pressure during the deposition are observed. In contrast, PL properties of highly porous films are mainly determined by post-deposition oxidation phenomena. They lead to an appearance and enhancement of PL bands around 1.6-1.7 eV and 2.2-2.3 eV, which are independent of the deposition conditions.

ACKNOWLEDGEMENTS

The authors are grateful to Prof. Richard Leonelli for assistance during PL measurements, Suzie Poulin for XPS measurements, and to Jean-Paul Levesque for technical assistance.

REFERENCES

1. L. A. Chiu, A. A. Seraphin, and K. D. Kolenbrander, "Gas Phase Synthesis and Processing of Silicon Nanocrystallites: Characterization by Photoluminescence Emission Spectroscopy", *J. Electron. Matter*, **23**, pp. 347-352, 1994.
2. D. B. Geohegan, A. A. Puretzky, G. Duscher, and S. J. Pennycook, "Time-resolved imaging of gas phase nanoparticle synthesis by laser ablation", *Appl. Phys. Lett.*, **72**, pp. 2987-2989, 1998.
3. E. Werwa, A. A. Seraphin, L. A. Chiu, C. Zhou, and K. D. Kolenbrander, "Synthesis and processing of silicon nanocrystallites using a pulsed laser ablation supersonic expansion method", *Appl. Phys. Lett.*, **64**, pp. 1821-1823, 1994.
4. I. A. Movtchan, R. W. Dreyfus, W. Marine, M. Sentis, M. Autric, G. Le Lay and N. Merk, "Luminescence from a Si-SiO_x nanocluster-like structure prepared by laser ablation", *Thin Solid Films*, **255**, pp. 286-289, 1995.
5. Y. Yamada, T. Orii, I. Umezu, Sh. Takeyama, and T. Yoshida, "Optical properties of silicon nanocrystallites prepared by excimer laser ablation in inert gas", *Jpn. J. Appl. Phys., Part 1*, **35**, pp.1361-1365, 1996.
6. T. Makimura, Y. Kunii, and K. Murakami, "Light emission from nanometer-sized silicon particles fabricated by the laser ablation method", *Jpn. J. Appl. Phys., Part 1*, **35**, pp.4780-4784, 1996.
7. T. Makimura, Y. Kunii, N. Ono, and K. Murakami, "Silicon nanoparticles embedded in SiO₂ films with visible photoluminescence", *Appl. Surf. Sci.*, **127-129**, pp. 388-392, 1998.
8. I. Umezu, K. Shibata, S. Yamaguchi, A. Sugimura, Y. Yamada and T. Yoshida, "Effects of thermal processes on photoluminescence of silicon nanocrystallites prepared by pulsed laser ablation", *J. Appl. Phys.*, **84**, pp. 6448-6450, 1998.
9. L. Patrone, D. Nelson, V. I. Safarov, M. Sentis, W. Marine, and S. Giorgio, "Photoluminescence of silicon nanoclusters with reduced size dispersion produced by laser ablation" *J. Appl. Phys.*, **87**, pp. 3829-3837, 2000.
10. A.V. Kabashin, M. Charbonneau-Lefort, M. Meunier, and R. Leonelli, "Effects of deposition and post-fabrication conditions on PL properties of nanostructured Si/SiO_x films prepared by laser ablation", *Appl. Surf. Sci.*, **168**, pp. 328-331, 2000.
11. A.V. Kabashin, M. Meunier, and R. Leonelli, "Photoluminescence characterization of Si-based nanostructured films produced by laser ablation", *J. Vac. Sci. Tech. B*, **19**, pp. 2217-2222, 2001.
12. L. T. Canham, "Silicon quantum wire array fabrication by electrochemical and chemical dissolution of wafers", *Appl. Phys. Lett.*, **57**, pp. 1046-1048, 1990.
13. Y. Kanemitsu, T. Ogawa, K. Shiraishi, and K. Takeda, "Visible photoluminescence from oxidized Si nanometer-sized spheres: exciton confinement on a spherical shell", *Phys Rev. B*, **48**, pp. 4883-4886, 1993.

14. S. M. Prokes, "Light emission in thermally oxidized porous silicon: Evidence for oxide-related luminescence", *Appl. Phys Lett*, **62**, pp. 3244-3246, 1993.
15. L. T. Parratt, "Surface studies of solids by total reflection of x-rays", *Phys. Rev.*, **95**, pp. 359-369, 1954.
16. D.H Lowndes, C.M Rouleau, T. Thundat, G. Duscher, E.A. Kenik, S.J. Pennycook, "Silicon and zinc tellurid nanoparticles synthesized by pulsed laser ablation: size distributions and nanoscale structure", *Appl. Surf. Sci.*, **127-129** pp. 355-361, 1998.
17. K.S. Min, K.V. Shcheglov, C.M. Yang, H.A. Atwater M.L. Brongersma, A. Polman, "Defect-related versus excitonic visible light emission from ion beam synthesized Si nanocrystals in SiO₂" *Appl. Phys. Lett.*, **69**, pp. 2033-2035 1996.
18. H. Tamura, M. Ruckschloss, T. Wirschem, S. Veptek, "Origin of the green/blue luminescence from nanocrystalline silicon", *Appl. Phys. Lett.*, **65**, pp. 1537-1539, 1994.
19. S. Munekuni, T. Yamanaka, Y. Shimogaichi, K. Nagasawa, Y. Hama, " Various types of nonbridging oxygen hole center in high-purity silicon glass", *J. Appl. Phys.*, **68**, pp. 1212-1217, 1990.
20. S. Botti, R. Coppola, F. Gourbilleau, R. Rizk, "Photoluminescence from silicon nano-particles synthesized by laser-induced decomposition of silane" *J. Appl. Phys.*, **88**, pp. 3396-3401, 2000.
21. S. Li, S. J. Silvers and M. S. El-Shall, "Surface oxidation and luminescence properties of weblike agglomeration of silicon nanocrystals produced by a laser vaporization-controlled condensation technique", *J. Phys. Chemistry B*, **101**, pp 1794-1802, 1997.